

Oxygen Ion Conduction in Oxide Materials: Selected Examples and Basic Mechanisms

L.S.M. TRAQEIA, F.M.B. MARQUES, V.V. KHARTON

Ceramics and Glass Engineering Department, CICECO
University of Aveiro, 3810-193 Aveiro, Portugal

Oxygen ion conductors with most symmetrical structures such as fluorite- and perovskite-related phases, rely on the mobility of oxygen vacancies. High-performance electrolytes, namely with the apatite type structure, recently developed, show dominant interstitial transport. In order to assess basic composition-conductivity relationships in a fluorite-derived C-type cubic structure with high tolerance to different types of oxygen defects, a series of Y_2O_3 -based materials were studied by impedance spectroscopy in air in the range 700-1000°C. Yttria doped with CaO exhibits reasonably high ionic conduction via the vacancy mechanism. Samples doped with ZrO_2 and HfO_2 possess oxygen interstitials as dominant defects, but show poor ionic conductivity when compared to Ca-doped materials. These tendencies, known for other fluorite-related phases such as pyrochlores, are opposite to those observed for apatite- and K_2NiF_4 -type structures. Comparison of ionic conductivity levels in various oxide materials suggests that fast interstitial migration may be expected for complex multicomponent materials where the ion transport occurs in lattice fragments with high bond ionicity. Furthermore, conduction-affecting stereological parameters, to a great extent, depend on the relaxation of covalent fragments.

Keywords: oxygen ion conductors, defect mobility, C-type cubic structure, yttria, apatite.

Conducción iónica del oxígeno en óxidos: mecanismos básicos y algunos ejemplos.

Los conductores iónicos de oxígeno con estructuras más simétricas como fluorita y perovskita dependen de la movilidad de las vacantes de oxígeno. Se han desarrollado recientemente electrolitos con elevadas prestaciones, los llamados de estructura tipo apatito, que muestran transporte intersticial dominante. Con el objeto de establecer las relaciones básicas entre composición y conductividad en una estructura cúbica tipo-C derivada de la fluorita con alta tolerancia a diferentes defectos de oxígeno, se han estudiado materiales basados en Y_2O_3 por espectroscopía de impedancia en el rango de temperaturas entre 700 y 1000°C. La yttria dopada con CaO exhibe una conductividad iónica razonablemente alta vía mecanismo de vacantes.

Las muestras dopadas con ZrO_2 y HfO_2 poseen oxígenos intersticiales como defectos dominantes pero presentan una conductividad iónica pobre comparada con los materiales dopados con CaO. Estas tendencias, conocidas para otras fases relacionadas con la estructura fluorita como los pirocloros, son opuestas a las que se observan en estructura de tipo apatito y K_2NiF_4 .

La comparación de los niveles de conducción iónica entre varios materiales oxídicos apunta a la existencia de un mecanismo rápido de migración intersticial. Este mecanismo cabría expresarse en materiales multicomponente complejos en los que el transporte iónico tiene lugar en partes de la red con elevada ionicidad del enlace. Más aún, los parámetros estereológicos que afectan a la conducción, en gran medida dependen de la relajación de las partes covalentes.

Palabras clave: conductores iónicos de oxígeno, movilidad de defectos, estructura cúbica tipo-C, yttria, apatito.

1. INTRODUCTION

Solid solutions, namely based on ZrO_2 , ThO_2 , HfO_2 , CeO_2 were extensively studied as oxygen-ion and mixed conducting materials, due to their potential application in several devices like solid oxide fuel cells, oxygen permeating membranes and potentiometric sensors (1-3). Besides their early discovery one century ago, in the late 50's and 60's a significant enthusiasm on this subject brought to the first line of attention materials mostly based on the fluorite and derived structures. One special example of derived structures includes sesquioxides like Y_2O_3 with the C-type cubic structure. Pyrochlores are another example of this kind. In general, to enhance the ionic conductivity of the base material, lower valence metal dopants were introduced. Oxygen vacancies formed to compensate for the dopant lower charge were found as the dominant mobile defects in most of these systems.

The relevance of all these materials justified one early

review with almost 700 references, by Etsell and Flengas, in 1970 (1). Recently, Skinner and Kilner published one comprehensive overview of the progress in this field (4), and significant differences can be noticed on the families of materials now mentioned. Besides the fluorite-related classical systems, we find now perovskites and perovskite-related structures (K_2NiF_4), but also the so-called BIMEVOX and LAMOX families of materials, ending with the apatites derived from $La_{10}(SiO_4)_6O_3$ and Ge-based analogues.

A comparison of all these materials can be found in several review papers (4,5). For former materials, the oxygen ion conduction mechanism was usually based on vacancies. In the case of apatites, the present understanding points towards an interstitial based mechanism (6-12).

To emphasize the novelty of recently developed ionic conductors with the apatite structure, this paper will start

with the presentation of recent results on the electrical properties of yttria-based solid solutions, with the C-type cubic structure. The sesquioxides with the C-type cubic structure, namely Y_2O_3 or Sc_2O_3 , show an unusual capability to form solid solutions with either divalent cations (e.g., Ca^{2+}) or tetravalent cations (e.g., Zr^{4+} or Hf^{4+}), with formation of oxygen vacancies or oxygen interstitials, respectively, to compensate for the different charge of the dopant cations with respect to the host. Previous work on these systems was based mostly on dc characterization techniques, (ac) constant frequency measurements, and lack of details on microstructural characterization. Lastly, previous work was also centered on single binary systems (e.g., Y_2O_3 -CaO), using specific sets of experimental techniques, hampering any reliable comparison between data obtained in different labs on different systems. An updated assessment of these systems with improved experimental tools seemed fully justified. This updated assessment is also expected to favor the understanding of the subsequent discussion on opposite tendencies observed in several families of materials with respect to defect mobility (vacancies versus interstitials).

The ultimate goal of this paper, however, is to try to use a series of own results on the C-type cubic structure and additional literature data on other systems and structures, to emphasize what we feel as a major development in this field. In fact, the discussion on oxygen ion conductors moved from reasonably simple models on key parameters with relevance on ionic mobility (mostly related to geometrical constraints), to a more complex level of treatment of ionic motion mechanisms. Furthermore, an almost "common feeling" on the need for oxygen vacancies to reach significant ionic conductivities was questioned in recent years.

2. EXPERIMENTAL

Y_2O_3 -based solid solutions, with either CaO, ZrO_2 or HfO_2 as dopants (up to 4 mol% cation dopant), were prepared by solid state reaction, starting from the corresponding oxides or carbonates. Repeated milling and calcination at $1000^\circ C$ of all components was used to favor the completeness of solid state reactions, due to the highly refractory characteristics of most components. Final sintering temperatures of $1600^\circ C$ were used in the case of undoped and Ca-doped samples, and $1700^\circ C$ in the case of Zr- and Hf-doped samples. Short designations will be used throughout this work to identify the nominal compositions under consideration. Accordingly, Y holds for undoped yttria, while xMY holds for $xMO_n \cdot (100-x)YO_{1.5}$ (e.g., $2ZrY = 2ZrO_2 \cdot 98YO_{1.5}$).

Sintered samples were characterized by XRD, SEM/EDS and impedance spectroscopy in air, in the frequency range 20 Hz to 1 MHz, up to $1000^\circ C$. Samples used in electrical measurements were previously electroded with porous Pt layers.

3. RESULTS

All materials used for electrical measurements were single-phase with the C-type cubic structure, according to XRD. However, in the case of Ca-doped samples, inspection by SEM complemented by EDS analysis, showed the presence of minor quantities of unreacted CaO grains. Selected examples

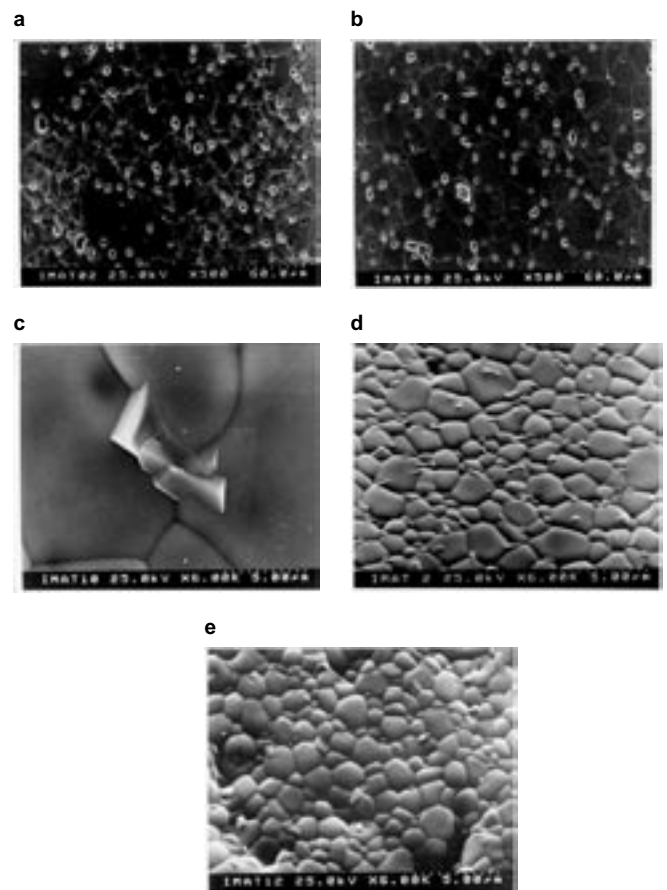


Fig. 1- Microstructures of yttria-based samples: a – 1CaY; b – 3CaY; c – detail of 3CaY showing the presence of a small grain of unreacted CaO; d – 1ZrY, e – 4ZrY.

of microstructures of some of the studied compositions, with emphasis on the presence of small CaO unreacted grains and residual porosity in the case of Ca-doped samples are shown in Fig. 1(a - c). Quite homogeneous microstructures of highly densified materials were obtained in the case of Zr-doped samples (Fig. 1(d) and 1(e)). Also, the average grain size of Ca-doped samples exceeds largely the average grain size of the Zr- and Hf-doped samples.

Figure 2 shows typical impedance spectra obtained for Ca-containing solid solutions. At lower temperatures, the high impedance of most samples prevented the identification of well defined spectra with high frequency, intermediate frequency, and low frequency arcs, as usual for such type of

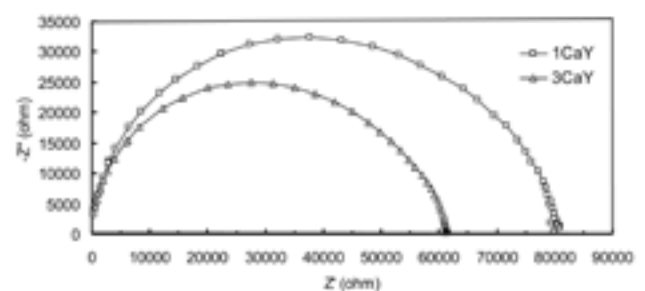


Fig. 2- Impedance spectra of Ca-doped yttria in air, at $700^\circ C$.

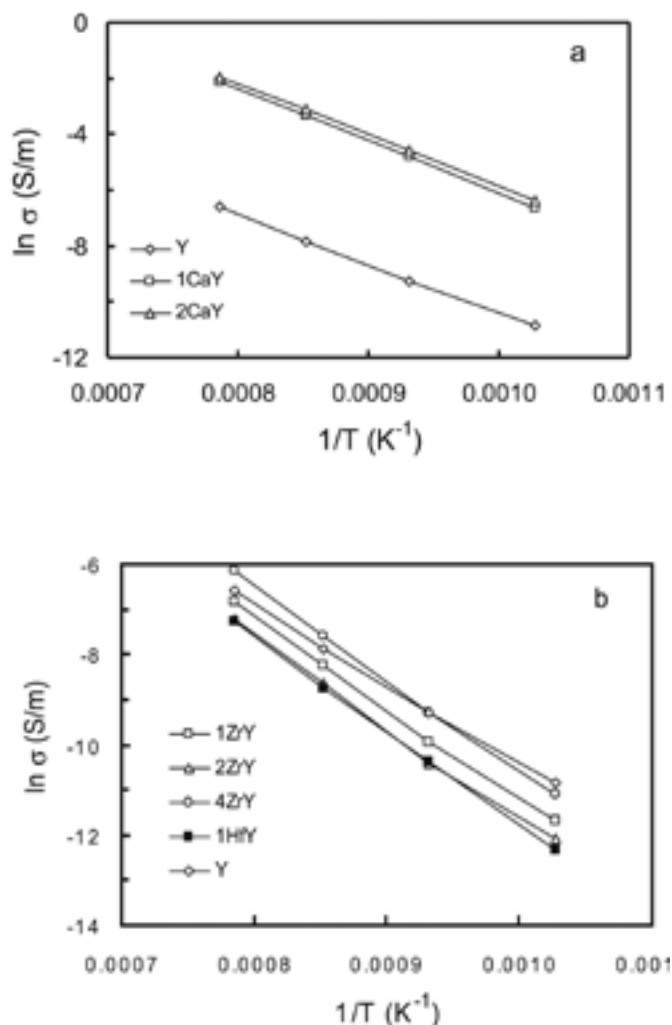


Fig. 3-Arrhenius-type plot of total conductivity versus the reciprocal of the absolute temperature, in air: a – undoped and Ca-doped samples; b – undoped, and Zr- and Hf-doped samples.

materials. This explains the emphasis on the discussion of relatively high temperature transport properties (700-1000°C).

Table 1 shows data obtained for the total conductivity in air of selected compositions studied in this work. The same results are also shown in Figure 3, as typical Arrhenius-type plots of $\ln \sigma$ versus $1/T$. The activation energies ranged between 137 kJ/mol for the undoped sample to 151 kJ/mol for the Ca-doped samples. For the Zr-doped samples the activation energy was in the range 162-170 kJ/mol. The activation energy of the Hf-doped sample was 170 kJ/mol. Some additional comments are needed on the results just presented.

Undoped yttria seems to show a reasonably high conductivity when compared to Zr- and Hf-doped materials. While we believe that the presentation of these results as a reference is fully justified, the magnitude of the observed conductivity is likely to be governed by the presence of minor impurities, or even influenced by the presence of protons. In fact, undoped yttria is highly sensitive to moisture, showing significant protonic conduction (13). From these comments we should conclude that the results just presented for undoped yttria are unlikely to correspond to the intrinsic behavior of this material. This means that direct comparison of these

results with data obtained for the remaining samples should be avoided without a deeper study on the possible presence and role of minor impurities and protons. None of these issues was further addressed for being outside the scope of this work.

Although data on undoped yttria should be considered with great care, the remaining sets of data show highly meaningful trends. Ca-doped samples exhibit conductivities about two orders of magnitude larger than those observed for the Zr- and Hf-doped samples, with similar dopant levels. In general, increasing dopant concentration has a positive effect on total conductivity.

A comparison of the present results with previously published data suggests, in general, a higher total conductivity for equivalent materials now prepared. One likely possibility is an improved processing route in the case of the present materials, with higher densifications and lower grain boundary and porosity related blocking effects. In general, this type of improvement should mostly enhance the ionic conductivity, as the electronic conductivity is usually less sensitive to such microstructural features. In fact, the presence of ion-blocking grain boundaries usually provides underestimated ionic transport numbers (14).

Previous studies on these systems already showed that these materials are mixed conductors in air, in the studied range of temperatures, with significant ionic transport numbers. Ionic conduction is thus believed to be dominant in most cases, considering the improved performance of the present materials.

The conductivity of solid solutions with tetravalent dopants is thus believed to be due mostly to interstitial oxygen ions formed to compensate for the excess charge of the dopant with respect to the host cation (e.g., $2[O_i^{\bullet\bullet}] = [Zr_Y^{\square}]$, using Kroger-Vink type notation). The ionic conductivity of materials with divalent dopants is due to oxygen vacancies, again formed to compensate for the different charge of the dopant with respect to yttrium ($[Ca_Y^{\prime}] = 2[V_O^{\square}]$). Both Zr- and Hf-doped samples show coherent levels of conductivity, suggesting negligible role of dopant size on the ionic transport properties of the solid solution. Ca-doped samples exhibit much higher

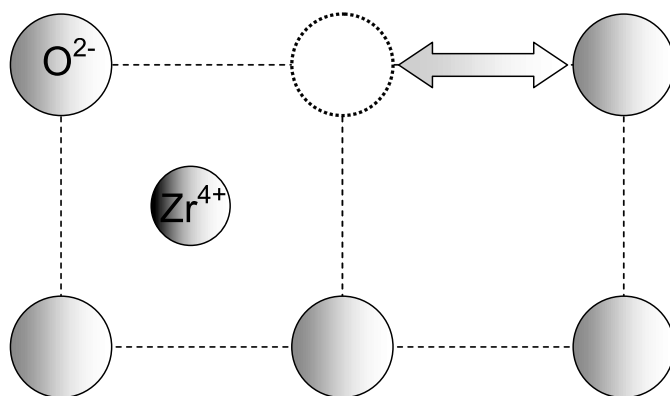


Fig. 4- Schematic view of the vacancy motion mechanism in the fluorite-type structure. Ionic positions are shown as filled circles, while the oxygen vacancy is shown as an empty circle within a dashed line. The metal cation is located below the plane containing the anions, in the center of a cube formed by eight oxygen ions/vacancies.

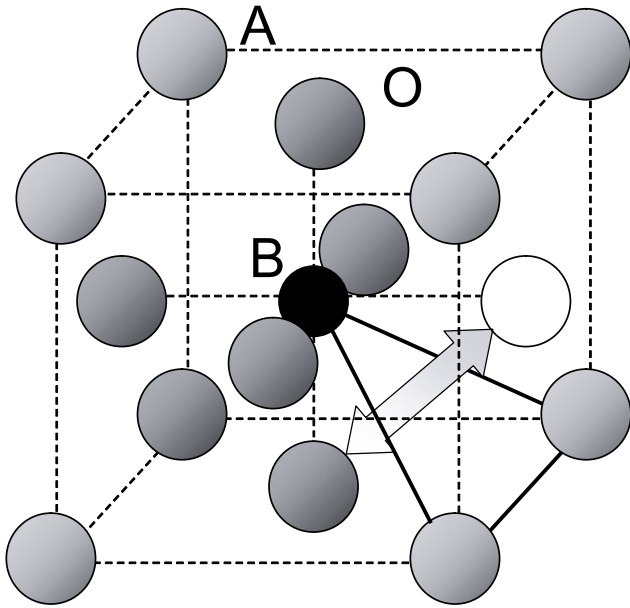


Fig. 5- Schematic view of the vacancy motion mechanism in perovskite-type structures. Ionic positions are shown as filled circles. The oxygen vacancy is shown as an empty circle. The triangle formed between two A- and one B- site cation is emphasized with a solid line.

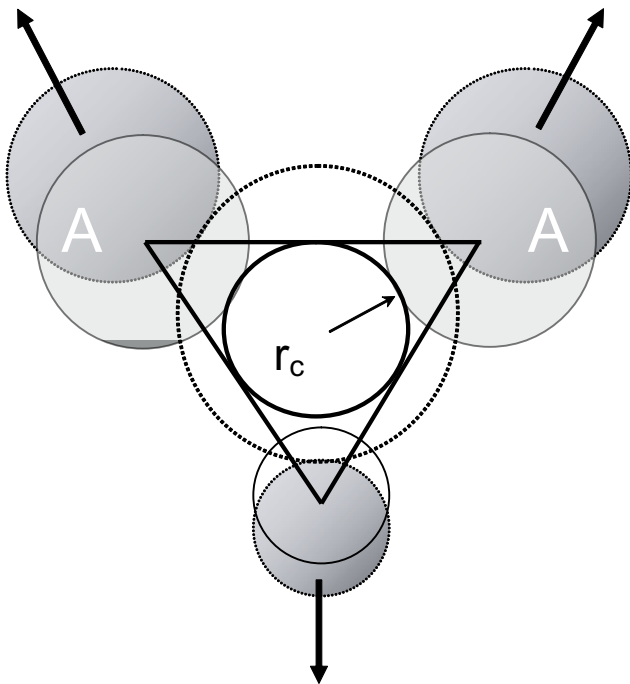


Fig. 6- Schematic view of the triangle formed by neighboring A- and B-site cations, through which oxygen ions must migrate. The apparent bottleneck has a critical radius r_c . Due to ionic relaxation from ideal positions (also suggested in the figure) and polarizability of the A- and B-site cations, the effective bottleneck is larger than simple estimates from lattice parameter and ionic radius.

TABLE I. TOTAL CONDUCTIVITY IN AIR OF SELECTED MATERIALS WITH THE C-TYPE CUBIC STRUCTURE.

T (°C)	σ (S/m)						
	Y	1CaY	3CaY	1ZrY	2ZrY	4ZrY	1HfY
700	2.0E-5	1.3E-3	1.7E-3	8.6E-6	5.7E-6	1.5E-5	4.4E-6
800	9.3E-5	8.2E-3	1.0E-2	4.9E-5	3.0E-5	9.3E-5	3.1E-5
900	3.8E-4	3.5E-2	4.5E-2	2.7E-4	1.7E-4	5.1E-4	1.6E-4
1000	1.4E-3	1.2E-1	1.4E-1	1.1E-3	7.1E-4	2.1E-3	7.0E-4

levels of conductivity, coherent with a much higher mobility for oxygen vacancies with respect to interstitials. This also points to slightly higher activation energy for ionic conduction when the mechanism for ionic motion is based on oxygen interstitials, again coherent with a larger jump distance, as explained in the following section, where the present results will be further used.

4. OXYGEN-ION CONDUCTION IN SOLID ELECTROLYTES: RELEVANT MECHANISMS

Yttria-stabilized zirconia (YSZ) is the best-known solid electrolyte with the fluorite structure. The ionic motion in fluorite based systems is the well established vacancy based mechanism, where one vacancy shifts position with a neighboring oxygen ion in a normal lattice position (Fig. 4). The easiest jump is along the edge of the cube formed by eight oxygen ions/vacancies. Optimization of oxygen transport in fluorite related systems can be based on simple considerations on dopant ionic size and charge, in combination with experimental data on phase relationships as a function of dopant content and temperature. Lattice distortion and strong defect association may be partly avoided if host cation and dopant have similar sizes and minimum charge difference. High concentrations of defects increase defect interaction and decrease the ionic conductivity (15,16). Highly-conductive perovskites derived from LaGaO_3 , usually doped with Sr in the A-site and Mg in the B-site, contain large concentrations of oxygen vacancies, the mobile defect involved in oxygen transport (17-24). The close packing of ions in this structure, leaves no room for formation of oxygen interstitial defects. In the case of perovskites, the most obvious pathway for oxygen ion hopping is through a triangle formed by two large A-cations and one small B-cation. The circle defined by this triangle was identified as the bottleneck for ionic transport (Figures 5 and 6). Assuming this pathway, simple relations between lattice parameters and cation sizes were derived, showing possible solutions to optimize the size of the above mentioned bottleneck and ionic conductivity (25). On the other hand, examples of deviation to this simple prediction are documented in the literature; one typical example is given in Table 1 (26). Ions do not behave as immobile hard spheres, and ionic polarizability and relaxation from ideal positions has also to be taken into consideration. Recent modeling on minimum energy pathways for ionic motion in this structure showed that oxygen ions indeed deviate from the expected ideal position, moving away from the center of the bottleneck formed by neighboring ions, due to relaxation of A- and B- cations from their ideal positions (Fig. 6). Also, due to different ionic polarizabilities, different cations adjust differently to this situation (27). In the case of Ag^+ ionic motion in AgI , besides the polarization of the large I ions, also the hybridization condition of Ag^+ changes to adjust the shape of

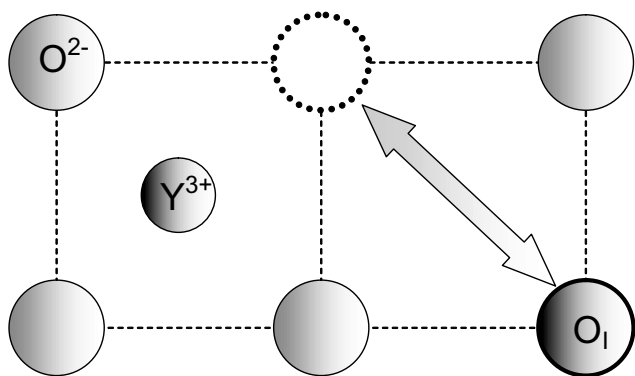


Fig. 7- Schematic view of the oxygen interstitial motion mechanism in the C-type cubic structure. Ion hopping is usually along face diagonals of the cubes defined by eight normal/interstitial oxygen positions. The occupied oxygen interstitial position is identified with the symbol "O₁". An empty interstitial position is shown as an empty circle surrounded by a dashed line. The metal cation is located below the plane containing the anions, in the center of a cube formed by eight oxygen ions/interstitial positions.

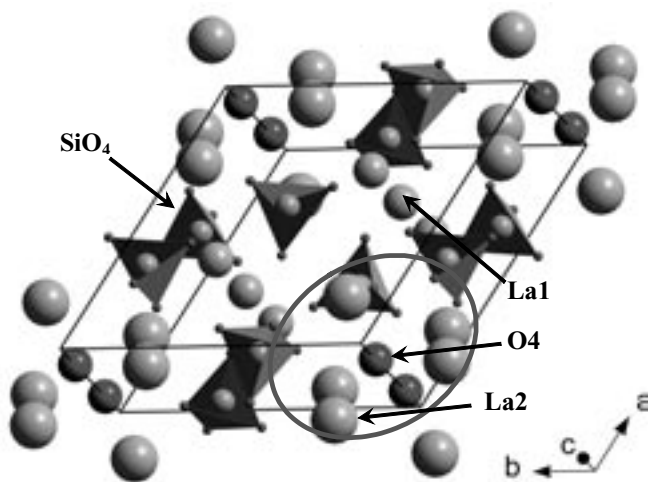


Fig. 8- Apatite structure of lanthanum silicate based materials with the positions of oxygen ions involved in the formation of interstitials identified as O4.

TABLE II. CRITICAL RADIUS, IONIC CONDUCTIVITY AT 800°C AND ACTIVATION ENERGY FOR IONIC CONDUCTION OF SELECTED PEROVSKITE TYPE MATERIALS (26)

Composition	Critical radius r_c (Å)	Ionic conductivity (S/m)	Activation energy (kJ/mol)
$\text{La}_{0.95}\text{Sr}_{0.05}\text{GaO}_3$	0.7511	3.6	60.3
$\text{La}_{0.95}\text{Sr}_{0.05}\text{AlO}_3$	0.9028	2.4E-1	111

the repulsive core to this critical condition during ion hopping (28). All these arguments explain the deviation between observed experimental transport parameters and bottleneck dimensions, simply derived from lattice parameters and ionic radius. While perovskites show specific features with respect to the fluorite type structure, due to a more complex ionic packing model, the oxygen transport mechanism is still based on vacancies, as previously mentioned.

We have just presented a series of results enhancing the unusual capability of C-type sesquioxides to form solid solutions with either divalent cations (e.g., Ca^{2+}) or tetravalent cations (e.g., Zr^{4+} or Hf^{4+}), with formation of oxygen vacancies or oxygen interstitials, respectively. The versatility of this structure derives from the existence of large interstitial

TABLE III. CONDUCTIVITY (800°C) AND ACTIVATION ENERGY OF SELECTED OXYGEN ION CONDUCTORS.

Composition	Structure	Ionic conductivity (S/m)	Activation energy (kJ/mol)	Ref.
8% Y_2O_3 -92% ZrO_2	F	4.5	91	(38)
$\text{Ce}_{0.8}\text{Gd}_{0.2}\text{O}_{2-\delta}$	F	8.7	73	(39)
$(\text{La}_{0.9}\text{Sr}_{0.1})_{0.98}\text{Ga}_{0.8}\text{Mg}_{0.2}\text{O}_{3-\delta}$	Pe	8.6	71	(40)
$\text{Gd}_{1.8}\text{Ca}_{0.2}\text{Ti}_2\text{O}_{7-\delta}$	Py	1.5	65	(41)
$\text{La}_{10}\text{Si}_5\text{FeO}_{26.5\pm\delta}$	A	2.3	81	(42)
$\text{La}_{8.83}\text{Si}_{5.5}\text{Al}_{1.5}\text{O}_{26.5}$	A	4.6	57	(43)

F-fluorite, Pe-perovskite, Py-pyrochlore, A-apatite

positions, similar in size to those occupied by the oxygen ions in normal positions. In fact, the C-type cubic structure can be described as derived from the fluorite, with one fourth of the anions missing (Fig. 4). The interstitial positions form a continuous network throughout the lattice, thus suggesting one easy pathway for interstitial motion (29).

As previously shown, the ionic conductivity of Ca-doped yttria is by far larger than the corresponding value observed for Zr- or Hf-doped Y_2O_3 . Besides our own results, previous literature data shows identical trends: 5×10^{-2} S/m versus 1.7×10^{-3} S/m, for 3% CaO -97% $\text{YO}_{1.5}$ and 5% CeO_2 -99% $\text{YO}_{1.5}$, respectively, at 1000°C (2,29). Earlier work on Sc_2O_3 -ZrO₂ and Y_2O_3 -HfO₂ showed always poor levels of ionic conduction, when compared to the equivalent results obtained with Ca-doped Y_2O_3 (30,31). Highly mobile oxygen interstitials seemed unlikely to be formed in oxide structures, even when stereological constraints are absent.

Lanthanum silicates with the apatite structure were recently found to exhibit high oxygen ion conductivity. The ideal stoichiometry for apatites with XO_4 tetrahedra is $(\text{M}_1, \text{M}_2)_{10}(\text{XO}_4)_6\text{Zr}_2$, with all sites fully occupied. $\text{La}_{10}(\text{SiO}_4)_6\text{O}_3$ is a key example of this new family of materials. When we compare this formula with the ideal apatite composition, we realize that the metal sites have excess positive charge, balanced in this case by one excess oxygen ion. As all normal lattice positions are fully occupied, this oxygen must occupy

an interstitial position.

$\text{La}_{10}(\text{SiO}_4)_6\text{O}_3$ structure consists of isolated SiO_4 tetrahedra with La^{3+} and the remaining O^{2-} ions aligned along specific crystal directions (Figure 8). Neutron powder diffraction studies indicate that these additional oxygen ions, independent of the SiO_4 tetrahedra, occupy both "normal" sites along the [001] direction of the crystal, and interstitial positions close to these ones. Furthermore, not all normal sites are occupied, suggesting the formation of oxygen vacancies together with interstitial defects. Note that a qualitatively similar situation is also characteristic of other structural groups exhibiting fast oxygen ion conduction, such as K_2NiF_4 type and cuspidine (32-36). In this case mobile interstitials are located in the lattice fragments with mainly ionic bonding and the diffusion path is

external to the metal-oxygen polyhedra with strongly covalent bonding.

Attempts to change the ionic conductivity of the apatite phases included replacement of Sr for La, La deficiency, and replacement of Al or Fe for Si. In general, materials with more than 26 oxygen atoms per formula unit exhibit quite large ionic conductivities. Also, compositions with La vacancies show higher conductivity than those without metal vacancies (6-12). Modelling performed on ionic motion in these materials, suggests that interstitial oxygen anions are the dominant charge carriers. Moreover, La deficiency apparently has an important role in the formation of interstitial oxygen defects, enhancing this process with respect to the metal stoichiometric materials. At the same time, the diffusion path is nonlinear and each ion jump is accompanied with a strong relaxation of SiO_4 tetrahedra (12). The latter feature, in combination with the co-existence of lattice fragments having a drastically different bond ionicity, is considered one of the most relevant differences between simple (e.g. C-type, pyrochlore) and more complex (e.g. apatite, K_2NiF -type) interstitial conductors.

As opposed to the case just discussed of yttria-based solid solutions, apatites with high concentrations of oxygen vacancies are poor ionic conductors. The oxygen content can be decreased by replacement of Sr for La in $\text{La}_{10}(\text{SiO}_4)_6\text{O}_3$. For a Sr/La ratio of 2/8 the stoichiometric apatite is obtained, with 26 oxygens per formula unit. For higher Sr/La ratios, the number of oxygens per formula unit becomes lower than 26, and the ionic conductivity drops by more than one order of magnitude. Modelling performed on these materials indeed suggests that oxygen vacancies are the dominant defects, although poorly mobile.

Comparison of the oxygen ion conductivity of these apatites with well-known oxygen ion conductors (Table 2) shows that we are in the presence of competitive materials, namely in the low-intermediate temperature range.

5. FINAL COMMENTS

While we are still in the presence of significant speculation on the structural features of apatites, including the suggested exact location of oxygen ions and ionic motion mechanisms, there is no doubt that an entirely new front was opened for further research. To a certain extent, recent work on novel structures with significant oxygen ion mobility had a precursor about 15 years ago, when the so-called C_{12}A_7 , a well-known calcium aluminate present in the cement chemistry, was studied by West and co-workers (37). The novelty of such a complex structure in the field of oxygen ion conductors deserved (and is yet likely to deserve) a deeper interest from the scientific community, again stressing the relevance of an enlargement of the field of study.

CONCLUSIONS

In the last 50 years promising oxygen ion conductors involved mostly vacancy based transport mechanisms. Exceptions to this case, where oxygen interstitials were tolerated, showed poor performance. The demonstration of high ionic conduction in the apatite structure, likely based on an interstitial mechanism, is to a reasonable extent one of the most relevant achievements in recent years, opening new directions for further research in this area.

REFERENCES

1. T.H. Etsell and S.N. Flengas, The Electrical Properties of Solid Oxide Electrolytes, *Chem. Rev.* 70, 339-376 (1970)
2. B.C.H. Steele, B.E. Powell and P.M.R. Moody, Anionic Conduction in Refractory Oxide Solid Solutions Possessing the Fluorite, Pyrochlore and Perovskite Structures, *Proc. Brit. Ceram. Soc.*, 10, 87-102 (1968)
3. B. Cales and J.F. Baumard, Conduction and Defect Structure of $\text{ZrO}_2\text{-CeO}_2\text{-Y}_2\text{O}_3$ Solid Solutions, *J. Electrochem. Soc.*, 131, 2407-2413 (1983)
4. S.J. Skinner and J.A. Kilner, Oxygen Ion Conductors, *Materials Today*, 30-37 (2003)
5. V.V. Kharton, F.M.B. Marques and A. Atkinson, Transport Properties of Solid Oxide Electrolyte Ceramics: a Brief Review, *Solid State Ionics*, 174, 135-149 (2004)
6. S. Nakayama, T. Kageyama, H. Aono, and Y. Sadaoka, Ionic Conductivity of Lanthanoid Silicates, $\text{Ln}_{10}(\text{SiO}_4)_6\text{O}_3$ (Ln = La, Nd, Sm, Gd, Dy, Y, Ho, Er and Yb), *J. Mater. Chem.*, 5, 1801-1805 (1995)
7. S. Nakayama and M. Sakamoto, Electrical Properties of New Type High Oxide Ionic Conductor $\text{RE}_{10}\text{Si}_6\text{O}_{27}$ (RE = La, Pr, Nd, Sm, Gd, Dy), *J. Eur. Ceram. Soc.*, 18, 1413-1418 (1998)
8. S. Tao and J.T.S. Irvine, Preparation and Characterisation of Apatite-Type Lanthanum Silicates by a Sol-Gel Process, *Mat. Res. Bull.*, 36, 1245-1258 (2001)
9. J.E.H. Sansom, D. Richings, and P.R. Slater, A Powder Neutron Diffraction Study of the Oxide-Ion-Conducting Apatite-Type Phases, $\text{La}_{9.33}\text{Si}_6\text{O}_{26}$ and $\text{La}_8\text{Sr}_2\text{Si}_6\text{O}_{26}$, *Solid State Ionics*, 139, 205-210 (2001)
10. J. McFarlane, S. Barth, M. Swaffer, J.E.H. Sansom, and P.R. Slater, Synthesis and Conductivities of the Apatite-type Systems, $\text{La}_{9.33+x}\text{Si}_{6-y}\text{M}_y\text{O}_{26+z}$ (M=Co, Fe, Mn) and $\text{La}_8\text{Mn}_2\text{Si}_6\text{O}_{26}$, *Ionics*, 8, 149-154 (2002)
11. A.L. Shaula, V.V. Kharton, J.C. Waerenborgh, D.P. Rojas, E.V. Tsipis, N.P. Vyshatko, M.V. Patrakeev and F.M.B. Marques, Transport Properties and Mossbauer Spectra of Fe-substituted $\text{La}_{10-x}(\text{Si,Al})_6\text{O}_{26}$ Apatites, *Mat. Res. Bull.*, 39, 763-773 (2004)
12. J.R. Tolchard, M.S. Islam and P.R. Slater, Defect Chemistry and Oxygen Ion Migration in the Apatite-Type Materials $\text{La}_{9.33}\text{Si}_6\text{O}_{26}$ and $\text{La}_8\text{Sr}_2\text{Si}_6\text{O}_{26}$, *J. Mater. Chem.*, 13, 1956-1961 (2003)
13. T. Norby, M. Videroe, R. Gloeckner and Y. Larring, Hydrogen in Oxides, *Dalton Trans.*, 3012-1018 (2004)
14. V.V. Kharton, F.M.B. Marques, E.V. Tsipis, A.P. Viskup, N.P. Vyshatko, M.V. Patrakeev, E.N. Naumovich and J.R. Frade, Interfacial Effects in Electrochemical Cells for Oxygen Ionic Conduction Measurements III. Transference Numbers vs. Grain-Boundary Resistivity, *Solid State Ionics*, 168, 137-151 (2004)
15. J.A. Kilner and B.C.H. Steele, Mass Transport in Anion-Deficient Fluorite Oxides, in *Nonstoichiometric Oxides*, Academic Press Inc., pp. 233-269 (1981)
16. E.C. Subbarao and H.S. Maiti, Solid Electrolytes with Oxygen Ion Conduction, *Solid State Ionics*, 11, 317-338 (1984)
17. T. Ishihara, H. Matsuda, and Y. Takita, Doped LaGaO_3 Perovskite Type Oxide as a New Oxide Ionic Conductor, *J. Am. Chem. Soc.*, 116, 3801-3803 (1994)
18. M. Feng and J.B. Goodenough, A Superior Oxide-ion Electrolyte, *Eur. J. Solid State Inorg. Chem.*, 31, 663-672 (1994)
19. P. Huang and A. Petric, Superior Oxygen Ion Conductivity of Lanthanum Gallate Doped with Strontium and Magnesium, *J. Electrochem. Soc.*, 143, 1644-1648 (1996)
20. J.W. Stevenson, T.R. Armstrong, D.E. McGready, L.R. Pederson, and W.J. Weber, Processing and Electrical Properties of Alkaline Earth-Doped Lanthanum Gallate, *J. Electrochem. Soc.*, 144, 3613-3620 (1997)
21. J. Drennan, V. Zelizko, D. Hay, F.T. Ciacci, S. Rajendran, and S.P. Badwal, Characterisation, Conductivity and Mechanical Properties of the Oxygen-ion Conductor $\text{La}_{9.9}\text{Sr}_{0.1}\text{Ga}_{0.8}\text{Mg}_{0.2}\text{O}_{3.87}$, *J. Mater. Chem.*, 7, 79-83 (1997)
22. R.T. Baker, B. Gharbage, and F.M.B. Marques, Ionic and Electronic Conduction in Fe and Cr Doped $(\text{La,Sr})\text{GaO}_3$, *J. Electrochem. Soc.*, 144, 3130-3135 (1997)
23. V.V. Kharton, A.P. Viskup, E.N. Naumovich, and N.M. Lapchuk, Mixed electronic and ionic conductivity of $\text{LaCo}(\text{M})\text{O}_3$ (M=Ga, Cr, Fe or Ni): I. Oxygen transport in perovskites $\text{LaCoO}_3\text{-LaGaO}_3$, *Solid State Ionics*, 104, 67-78 (1997)
24. T. Ishihara, M. Higuchi, H. Furutani, T. Fukushima, H. Nishiguchi and Y. Takita, Potentiometric Oxygen Sensor Operable in Low-Temperature by Applying LaGaO_3 -Based Oxide for Electrolyte, *J. Electrochem. Soc.*, 144, L122-125 (1997)
25. J.A. Kilner, R.J. Brook, A Study of Oxygen Ion Conductivity in Doped Non-Stoichiometric Oxides, *Solid State Ionics*, 6, 237-252 (1982)
26. P.S. Anderson, G.C. Mather, F.M.B. Marques, D.C. Sinclair, A.R. West, Synthesis and Characterisation of $\text{La}_{0.95}\text{Sr}_{0.05}\text{GaO}_{3.87}$, $\text{La}_{0.95}\text{Sr}_{0.05}\text{AlO}_{3.8}$ and $\text{Y}_{0.95}\text{Sr}_{0.05}\text{AlO}_{3.87}$, *J. Eur. Ceram. Soc.*, 19, 1665-1673 (1999)
27. M.S. Islam, Computer Modelling of Defects and Transport in Perovskite Oxides, *Solid State Ionics*, 154-155, 75-85 (2002)
28. J.B. Goodenough, *Solid Electrolytes, Pure and Applied Chemistry*, 67, 931-938 (1995)

29. F.M.B. Marques, G.P. Wirtz, Electrical Properties of Ceria-Doped Yttria, *J. Am. Ceram. Soc.*, 74, 598-605 (1991)
30. Z.S. Volchenkova, V.M. Nedopekin, Study of the Defect Structure of Sc_2O_3 , *Izv. Akad. Nauk SSSR, Neorg. Mat.*, 12, 1820-1823 (1976)
31. Z.S. Volchenkova, D.S. Zubankova, Electric Conductivity and Mobility of Oxygen Ions in Yttrium Oxide Containing Small Additions of Hafnium Oxide, *Izv. Akad. Nauk SSSR, Neorg. Mat.*, 14, 2211-2215 (1978)
32. V.V. Kharton, A.P. Viskup, A.V. Kovalevsky, E.N. Naumovich and F.M.B. Marques, Ionic Transport in Oxygen-hyperstoichiometric Phases with K_2NiF_4 -type Structure, *Solid State Ionics* 143, 337-353 (2001)
33. J.M. Bassat, P. Odier, A. Villesuzanne, C. Marin and M. Pouchard, Anisotropic Ionic Transport Properties in $\text{La}_2\text{NiO}_{4+\delta}$ Single Crystals, *Solid State Ionics*, 167, 341-347 (2004)
34. O. Joubert, A. Magrez, A. Chesnaud, M.T. Caldes, V. Jayaraman, Y. Piffard and L. Brohan, Structural and Transport Properties of a New Class of Oxide Ion Conductors: $\text{Nd}_4[\text{Ga}_{2(1-x)}\text{M}_{2x}\text{O}_{7+x}\text{O}_{1-x}]_2$ ($\text{M}=\text{Ti}, \text{Ge}$), *Solid State Sci.*, 4, 1413-1418 (2002)
35. A. Chesnaud, O. Joubert, M.T. Caldes, S. Ghosh, Y. Piffard and L. Brohan, Cuspidine-like Compounds $\text{Ln}_4[\text{Ga}_{2(1-x)}\text{Ge}_{2x}\text{O}_{7+x}\text{O}_{1-x}]_2$ ($\text{Ln} = \text{La}, \text{Nd}, \text{Gd}; x \leq 0.4$), *Chem. Mater.*, 16, 5372-5379 (2004)
36. M.C. Martin-Sedeno, E.R. Losilla, L. Leon-Reina, S. Bruque, D. Marrero-Lopez, P. Nunez and M.A.G. Aranda, Enhancement of Oxide Ion Conductivity in Cuspidine-type materials, *Chem. Mater.*, 16, 4960-4968 (2004)
37. M. Lacerda, J.T. Irvine, F.P. Glasser, A.R. West, High Oxide Ion Conductivity in $\text{Ca}_{12}\text{Al}_{14}\text{O}_{39}$, *Nature*, 332, 525-526 (1988)
38. M. Mori, T. Abe, H. Itoh, O. Yamamoto, Y. Takeda, T. Kawahara, Cubic-Stabilized Zirconia and Alumina Composites as Electrolytes in Planar Type Solid Oxide Fuel Cells, *Solid State Ionics* 74, 157-164 (1994)
39. V.V. Kharton, A.P. Viskup, F.M. Figueiredo, E.N. Naumovich, A.A. Yaremchenko, F.M.B. Marques, Electron-Hole Conduction in Pr-doped $\text{Ce}(\text{Gd})\text{O}_{2-\delta}$ by Faradaic Efficiency and Emf Measurements, *Electrochim. Acta* 46, 2879-2889 (2001)
40. V.V. Kharton, A.L. Shaula, N.P. Vyshatko, F.M.B. Marques, Electron-Hole Transport in $(\text{La}_{0.9}\text{Sr}_{0.1})_{0.98}\text{Ga}_{0.08}\text{Mg}_{0.02}\text{O}_{3.8}$ Electrolyte: Effect of Ceramic Microstructure, *Electrochim. Acta* 48, 1817-1828 (2003)
41. S.A. Kramer, H.L. Tuller, A Novel Titanate-based Oxygen Ion Conductor: $\text{Gd}_2\text{Ti}_5\text{O}_{15}$, *Solid State Ionics* 82, 15-23 (1995)
42. V.V. Kharton, A.L. Shaula, M.V. Patrakeev, J.C. Waerenborgh, D.P. Rojas, N.P. Vyshatko, E.V. Tsipis, A.A. Yaremchenko, F.M.B. Marques, Oxygen Ionic and Electronic Transport in Apatite-type Solid Electrolytes, *J. Electrochem. Soc.*, 151, A1236-1246 (2004)
43. A.L. Shaula, V.V. Kharton, F.M.B. Marques, Oxygen Ionic and Electronic Transport in Apatite-type $\text{La}_{10-x}(\text{Si},\text{Al})_6\text{O}_{26+3\delta}$, *J. Solid State Chem.*, 178, 2050-2061 (2005)

Recibido: 15.07.05

Aceptado: 14.02.06

